Measuring local thermal conductivity in polycrystalline diamond with a high resolution photothermal microscope

J. Hartmann, P. Voigt, and M. Reichling[a)]
Freie Universität Berlin, Fachbereich Physik, 14195 Berlin, Germany

(Received 21 June 1996; accepted for publication 27 November 1996)

A photothermal microscope that provides micrometer lateral and submicrometer depth resolution was designed. Thermal conductivity measurements with modulation frequencies up to 12 MHz on single grains in polycrystalline diamond demonstrate its lateral resolution power even for a highly conducting material. Measured conductivities strongly depend on the averaged volume and values up to 2200 W/mK are found in the high frequency limit where the properties inside a grain are sampled. The capability of the instrument to measure thermal parameters on thin films is demonstrated for gold films evaporated on quartz with a thickness ranging from 20 to 1500 nm. Measurements reveal a strong thickness dependence for both thin film conductivity and the contact resistance between film and substrate. Thermal conductivity decreases monotonically from 230 to 30 W/mK whereas the contact resistance rises from 2×10^{-7} to 8×10^{-6} m^2K/W with decreasing film thickness. © *1997 American Institute of Physics.* [S0021-8979(97)00906-7]

I. INTRODUCTION

Photothermal microscopy was developed for both the measurement of thermal parameters with high spatial resolution[1] and for imaging applications[2,3] and the technique is now widely used in semiconductor material engineering.[4–12] Also for the characterization of inhomogeneous materials, mirage[13,14] and thermoreflectance[15,16] microscopes have successfully been used. New materials, like highly conductive chemical vapor deposited (CVD) diamond,[17] are a challenge with regard to lateral resolution and have stimulated further development of the technique.[18,19] In the present work we report about a photothermal microscope with a high bandwidth that provides a spatial resolution variable over a very large range. Integration of the setup into a commercial microscope and using highest modulation frequencies up to 12 MHz yield micrometer resolution even for highly conducting materials. In contrast to heterodyne techniques[20,21] where high frequency thermal or acoustic signals are mixed and detected at their difference frequency, here we utilize a double modulation technique capable of detecting small high frequency signals on a strong coherent background by two-stage LockIn detection. The large scanning area of the pump beam with respect to the probe beam of up to 0.25 mm^2 allows thermal parameter measurements with high accuracy. The capabilities of the instrument are demonstrated for two typical applications. High resolution measurements on CVD diamond reveal information about heat flow in single diamond grains, while measurements on a set of thin gold films of 20–1500 nm thickness provide precise data for thickness-dependent thermal conductivity and contact resistance between film and substrate. In Sec. II we describe the experimental setup in detail. In an extension of a previously published theory[22] we present a simple formula for the calculation of thermal diffusivity and contact resistance in Sec. III. Results for the measurements on CVD diamond and gold films are presented and discussed in Secs. IV and V, respectively.

II. EXPERIMENT

The experimental setup is shown schematically in Fig. 1. To obtain highest local resolution we aimed for an optimization of both laser spot sizes and thermal diffusion length. To achieve high optical resolution the photothermal apparatus was integrated into a commercial microscope (Carl Zeiss Jenavert), yielding focal diameters very close to the diffraction limit for the laser beams.

The sample is mounted on a two-dimensional translation stage and can be positioned with 0.1 μm precision. A dichroic mirror is used to combine the HeNe laser probe beam with the Ar^+ laser pump beam and both pass a polarizing beam splitter and a $\lambda/4$ plate before they are focused onto the sample surface by the microscope objective. The pump laser power incident on the sample can be controlled by the Ar^+ laser and was kept below 100 mW while the probe laser had a power below 5 mW. Having passed the $\lambda/4$ plate two times the reflected HeNe laser beam passes straight through the beam splitter and is focused onto a photodetector after separation from the Ar^+ laser beam by an interference filter. A movable lens in the heating laser beam path is used to adjust the relative positions of the pump and probe beams on the sample surface from 0 to 500 μm.

The Ar^+ laser beam is modulated with an acousto-optic modulator (A&A MTO8) and, when using double modulation, additionally with a mechanical chopper (HMS model 221) operated at 3.5 kHz. The upper limit of 12 MHz for the high frequency is set by the HF-LockIn amplifier (single-phase LockIn, Princeton Applied Research PAR100) while the ac-coupled preamplifier (analog modules 312) connected to the photodetector defines the bandwidth limit on the low frequency side at 100 Hz. For high frequency operation (frequencies larger than 1 MHz) a double-modulation technique[23] is used that is capable of eliminating any electromagnetic pickup at the frequency of photothermal modu-

[a)]Corresponding author. Electronic mail: reichling@matth1.physik.fu-berlin.de

 0021-8979/97/81(7)/2966/7/$10.00

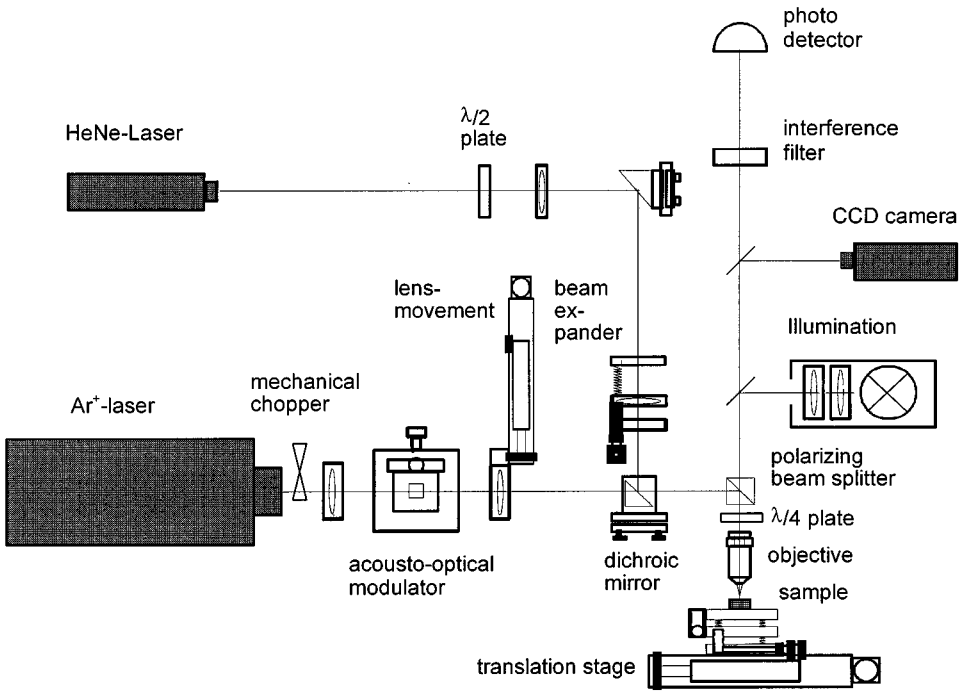

FIG. 1. Schematic view of the photothermal microscope.

lation (e.g., stray fields from the acousto-optic modulator) that would otherwise be a major source of an unwanted signal when working with MHz frequencies. The amplified detector signal is first analyzed by the HF-LockIn amplifier synchronized to the high frequency of the acousto-optical modulator. The output signal of this LockIn is filtered with a 3 μs time constant and still carries the modulation from the mechanical chopper. This low frequency signal is rectified by the second LockIn (dual-phase LockIn, EG&G 5210) referenced to the 3.5 kHz modulation (chopper) and operated in the amplitude/phase mode with a time constant of typically 300 ms. The output signal of the second LockIn represents the amplitude of the low frequency signal that in turn is proportional to the amplitude of the high frequency signal times the cosine of the phase difference between the high frequency reference and photothermal signals. As the high frequency LockIn is only a single-phase instrument, one has to measure the amplitude for at least two different reference phases to obtain complete information about the amplitude and phase of the high frequency photothermal signal. To enhance the accuracy of the measurements the phase of the high frequency reference is shifted in eight steps from 0° to 360° and the amplitude of the low frequency signal is recorded as a function of these phase shifts. Amplitude and phase of the high frequency photothermal signal are determined by a fit of a sine function to this data. Any high frequency stray field at the photothermal modulation frequency picked up by the sensitive electronics would also be measured when using only the HF-LockIn for signal detection. By additionally modulating the pump laser beam with the low frequency and inserting the second LockIn, such unwanted signals are effectively filtered out since they appear as a constant voltage at the output of the HF-LockIn and are suppressed by the second LockIn while the wanted photothermal signals pass. Of course, there is also a strong photothermal response to the 3.5 kHz modulation from the chopper. However this can safely be ignored since it is linearly superimposed to the high frequency signal and effectively suppressed by the HF-LockIn. Furthermore, the thermal decay length for the 3.5 kHz signal is more than one order of magnitude larger than the length for the high frequency signal and, therefore, no significant phase shift or amplitude change has to be expected over the distances scanned in this experiment.

III. THEORY

Thermal diffusivity measurements of isotropic bulk materials involve thermal waves $T \propto \exp(iqr - i\omega t)/r$, where r is the radial distance from the heating source, and the dispersion relation,[24]

$$q^2 = \frac{i\omega}{D}, \tag{1}$$

defines the wave number q depending on thermal diffusivity D and modulation frequency $\omega = 2\pi f$. Measuring the phase lag of the thermal wave $\Delta\phi = (\omega/2D)^{1/2}\Delta x$ at a distance Δx from the excitation allows a straightforward determination of thermal diffusivity.

To describe thermal waves in thin film systems in general, one has to solve the heat diffusion equation in all constituents and combine solutions by appropriate boundary conditions.[25] Recently we have shown,[22] however, that, in the case of an optically thick but thermally thin film, the calculation can substantially be simplified by solving the heat diffusion equation for the substrate alone by applying a

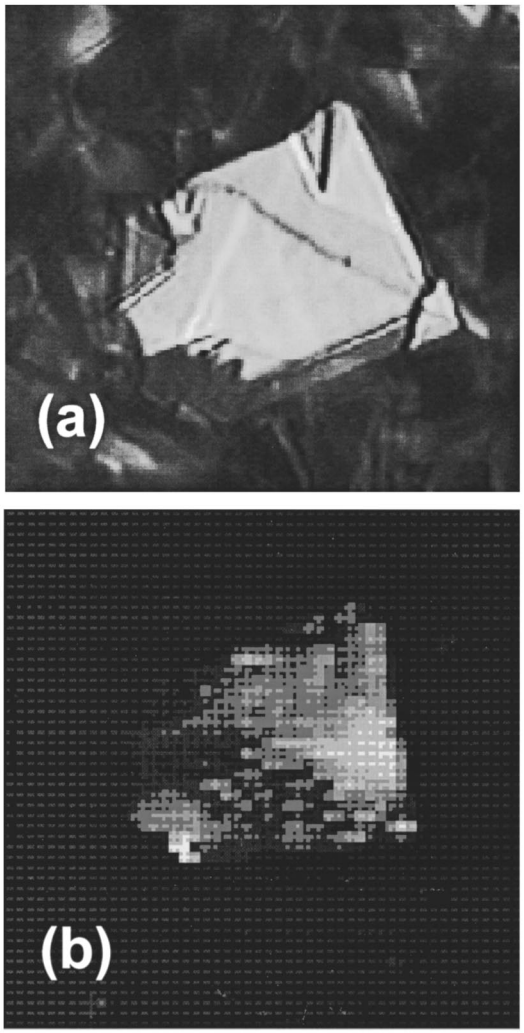

FIG. 2. (a) Microscopy image of a large CVD diamond grain. The grain is one of the few on the as-grown sample with a flat surface parallel to the scanning direction and, therefore, easily accessible for the photothermal investigation. (b) Photothermal amplitude recorded with 60 kHz modulation frequency when scanning over this grain. The area shown is 60×60 μm^2 in both images.

modified boundary condition. We use this approach for the analysis of data presented below but take additional thermal resistance between film and substrate into account. The modified calculation is outlined in the Appendix and yields an implicit equation for q:

$$\frac{i\omega}{D_f}-q^2=\frac{\kappa_s}{h\kappa_f}\frac{\left(q^2-\frac{i\omega}{D_s}\right)^{1/2}}{1+\kappa_s R_{\mathrm{th}}\left(q^2-\frac{i\omega}{D_s}\right)^{1/2}}, \tag{2}$$

where κ is the thermal conductivity, h the film thickness, and R_{th} the thermal resistance between film and substrate. The subscripts f and s denote parameters for the film and substrate, respectively. By measuring the phase lag $\Delta\phi$ of the thermal wave as a function of the distance Δx from the heating source on the sample surface, thermal diffusivity and contact resistance at the interface can be extracted using the relation

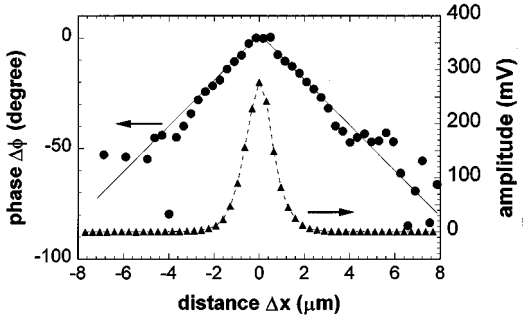

FIG. 3. Amplitude and phase profiles recorded on a large CVD diamond grain of a polished sample at a modulation frequency of 12 MHz. The solid line is a fit to the isotropic heat flow model assuming a bulk conductivity of 2200 W/mK.

$$\mathrm{Re}(q)=\frac{\Delta\phi}{\Delta x}. \tag{3}$$

This is done by a least-square procedure fitting parameters in Eq. (2) to the measured values for the distance dependent phase lag.

IV. THERMAL CONDUCTIVITY OF CVD DIAMOND GRAINS

To demonstrate the importance of high lateral resolution for a local thermal analysis we first present a measurement on a single CVD diamond grain. As can be seen in the microscopy image of Fig. 2(a), this grain appears as a markedly regular area on the as-grown surface of a polycrystalline sample that was covered with a thin layer of gold to assure homogeneous absorption of the pump laser light. During this measurement pump and probe laser beams were focused onto the same spot and the sample was scanned. The resulting photothermal amplitude image over an area of 60×60 μm^2 at 60 kHz modulation frequency is shown in Fig. 2(b). Except for some steps, the surface of the grain is rather smooth, as is evident from the optical image, and it was also checked by recording the total reflectivity of the probe beam during the photothermal scan. In contrast, the photothermal amplitude image reveals substantial structures. The location of the two hot spots in the lower left corner and close to the right edge in particular cannot be inferred from the optical image. Presumably they indicate the location of hidden thermal boundaries inside the grain or areas of high defect concentration. This example clearly demonstrates that for any measurement aimed at measuring thermal conductivity inside a grain the laser beam has to be positioned very carefully and the measured heat flow has to be restricted to a thermally active volume of the order of 100 μm^3.

To measure thermal conductivity within such grains, we applied the photothermal profile analysis described in detail elsewhere.[26,27] Due to the high thermal conductivity within the diamond grain very high modulation frequencies are necessary to restrict the measured heat flow to a single grain. Typical amplitude and phase profiles of the surface temperature obtained on a polished CVD diamond tile of 590 μm thickness at a frequency of 12 MHz are shown in Fig. 3. Note that there is a very high amplitude in the center region

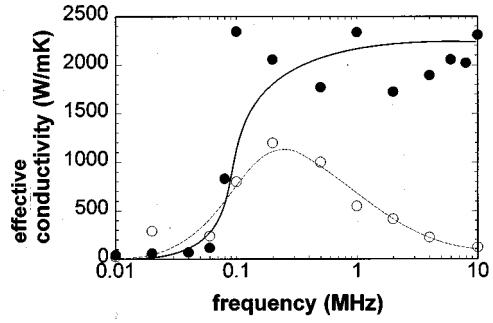

FIG. 4. Thermal conductivity of a CVD diamond sample extracted by beam profile analysis (see Fig. 3) for different modulation frequencies. Closed circles show results extracted from measurements on a sample with a 20 nm gold surface layer, while open circles represents results for a 70 nm gold/chromium surface layer.

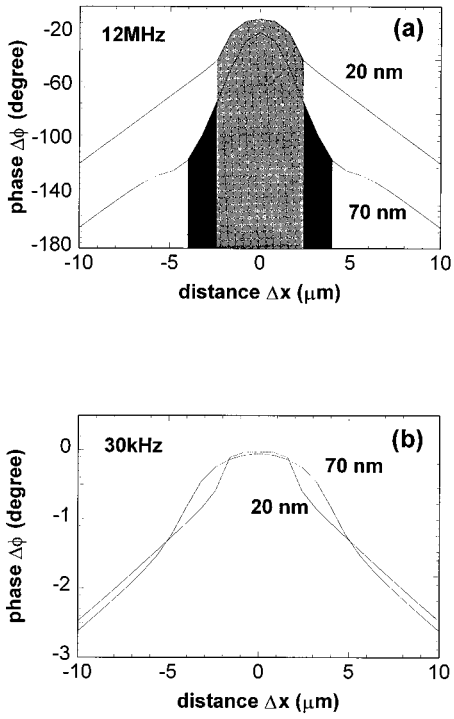

FIG. 5. Theoretical calculations of the phase lag at (a) 12 MHz and (b) 30 kHz modulation frequency for a gold film on diamond. The curves represent results for 20 nm layer thickness with $\kappa_{gold}=30$ W/mK and $R_{th}=5\times10^{-8}$ m^2 K/W and results for 70 nm with $\kappa_{gold}=80$ W/mK and $R_{th}=5\times10^{-8}$ m^2 K/W. The shaded regions in (a) show the distance ranges most affected by the gold layer.

that is directly heated by the pump beam and a slow diffusive decay further outside. The high sensitivity of our instrument allows measurements far beyond the heated region (i.e., up to 5 μm for a 1 μm pump beam radius for the measurement shown in Fig. 3) and, therefore, provides a very reliable analysis of the phase profiles.

Averaged conductivities for a range of frequencies extracted by profile analysis using the model for isotropic heat flow are shown in Fig. 4. Beam profile analysis yields a thermal conductivity averaged over the thermally active volume determined by the thermal diffusion length $L_{th}=(2D/\omega)^{1/2}$. Therefore performing measurements in the middle of a large CVD diamond grain should yield increasing thermal conductivity with increasing modulation frequency. The solid curve in Fig. 4 shows that, for a large grain already at a frequency of 100 kHz, a conductivity of 2200 W/mK, i.e., a diamond bulk value,[28] can be measured and a further increase in frequency yields the same value except for some scatter due to sample inhomogeneity. These measurements were taken on a sample where the absorbing gold film was extremely thin (approximately 20 nm) and the pump beam was partly transmitted by the gold layer, resulting in low absorption and, therefore, a small signal amplitude. Due to the high transparency of the diamond tile the bulk absorption of the transmitted pump laser light does not contribute significantly to sample heating and the assumption of pure surface heating is still valid. The situation is different for samples covered with a thicker gold film. There, the pump beam is completely absorbed within the layer resulting in much less scattered data. However, as shown by the dashed curve in Fig. 4, the thicker gold layer (approximately 70 nm) introduces a significant systematic error at high frequencies, i.e., samples with a thicker gold layer yield reduced thermal conductivity.

To explain this phenomenon we recall that using higher modulation frequencies for photothermal analysis results in an enhanced surface sensitivity.[29] Consequently the influence of the thermal properties of the gold film gains importance. On the other hand, it is well known that gold films have a polycrystalline structure[30,31] that results in reduced thermal conductivity with decreasing film thickness.[26,32] The poor adhesion of the films on dielectric materials is also described in the literature.[33] If the thickness of the gold layer and the thermal resistance at the gold/diamond interface exceed critical values (approximately 30 nm and 1×10^{-8} m^2K/W), the influence of the gold film is no longer negligible. To confirm this we performed model calculations using a rigorous three-dimensional theory for a thin film on a substrate system.[25] Theoretical phase profiles for 20 and 70 nm gold films on diamond at 30 kHz and 12 MHz modulation frequency are shown in Fig. 5. The values for film conductivity and thermal resistance are taken from precise measurements of thin gold films on quartz substrates that are presented below. As can clearly be seen, the change in the slope of the phase profile introduced by the gold film is much more significant in the case of the 12 MHz simulations. Data analysis based on measuring the slope in a region of about 8 μm around the center is much less affected in the case of a measurement at 30 kHz modulation frequency. However, this frequency is much too low for local thermal analysis. In conclusion it can be said that highly resolved thermal measurements require strict high modulation frequencies and very thin metal overlayers and a reliable data analysis is fostered by measuring phase profiles over a large distance.

V. THERMAL CONDUCTIVITY OF GOLD FILMS

The aforementioned considerations show that the influence of the gold layer is a crucial question and potential

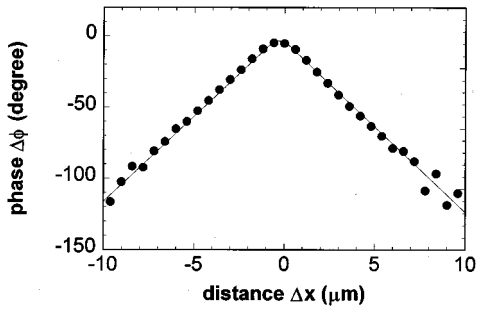

FIG. 6. Photothermal phase profile for a 100 nm gold film on quartz measured at a frequency of 1 MHz. The solid line is a fit of the theoretical model [Eq. (2)] to the experimental data. The fit yields 100 W/mK and 5×10^{-7} m^2K/W for thermal conductivity and thermal resistance, respectively. The thermal conductivity of the quartz substrate (1 W/mK) was inserted as a fix parameter.

obstacle for local conductivity measurements. We therefore investigated thermal properties of thin gold films on a dielectric substrate in some detail. In a previous publication we had demonstrated that the thickness of gold films has a strong influence on their thermal properties.[26] To determine thermal conductivity and contact resistance to the substrate precisely as a function of thickness we revisited the problem by measuring a set of gold films evaporated on fused silica substrates in the thickness range of 20–1500 nm. For the present investigation we used essentially the same method as described previously,[26] however, the considerably smaller focal diameters of the pump and probe beams that could be obtained with the new photothermal microscope dramatically reduced convolution effects and, therefore, greatly enhanced the precision of the profile analysis and allowed for the use of the simple model calculation. Figure 6 demonstrates that the resulting phase profiles are essentially straight lines and very precise values for their slope can be extracted.

To minimize experimental uncertainty, we performed measurements at four different modulation frequencies, 0.05, 0.2, 0.5, and 1 MHz. Values for thermal conductivity and thermal resistance were extracted from the measured phase curves using Eq. (2) and the results are shown in Figs. 7(a) and 7(b). It is important to note that a theoretical model neglecting the thermal contact resistance between film and substrate is not able to fit measurements at all frequencies. As expected, we found thin film conductivity decreasing with film thickness with the lowest value more than one order of magnitude below the bulk value whereas thermal resistance exhibits the opposite tendency. Within the limit of large layer thickness the resulting thermal resistance is very close to the value obtained for a similar system, i.e., a 2-μm-thick gold layer on silicon oxide.[33] The reduction of thermal resistance with increasing layer thickness is probably due to annealing effects at the interface during longer sputter times. From this and other observations[32] we anticipate that the thermal properties of the gold films obtained are quite universal and not restricted to systems prepared for the present investigation.

The solid curve shown in Fig. 7(a) is a fit to the empirical formula[34]

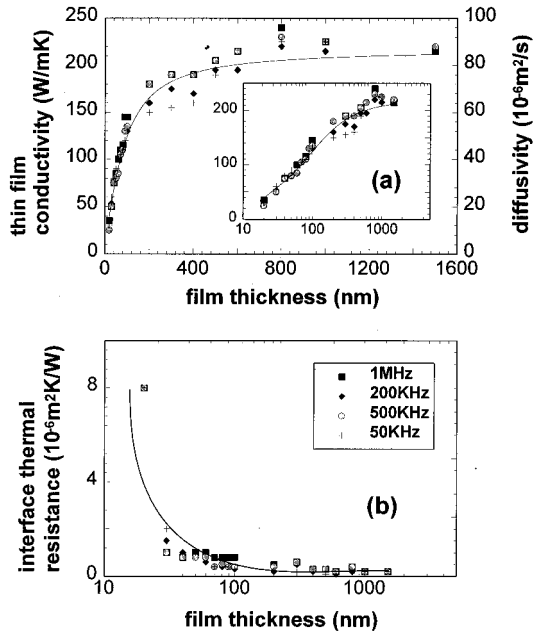

FIG. 7. (a) Measured thermal conductivity of gold films as a function of film thickness. The solid line is a fit to Eq. (3). The inset displays the same data on a logarithmic thickness scale. Different symbols represent results obtained for various frequencies and are defined in the inset of (b). (b) Thermal resistance between gold film and quartz substrate vs film thickness. The solid line is a guide to the eye.

$$\kappa_{\mathrm{eff}}=\kappa(0)+[\kappa(\infty)-\kappa(0)]\left\{1+\frac{z_0}{z}[\exp(-z/z_0)-1]\right\}, \tag{4}$$

with $\kappa(\infty)$ being the limiting thermal conductivity value for infinite film thickness, while $\kappa(0)$ is the value for zero film thickness. The fit gives a thermal conductivity $\kappa(\infty)=(219\pm5)$ W/mK which is considerably below the bulk thermal conductivity of gold, $\kappa_{\mathrm{gold}}=310$ W/mK.[35] This fact can be ascribed to the well known polycrystalline structure of gold films,[30,31,36] where the boundaries between the single grains act as an additional thermal resistance lowering the overall thermal conductivity measured in our experiments. The resulting $\kappa(0)=0.5$ W/mK represents the thermal conductivity for an infinitely thin layer of gold at the early stage of the deposition. Assuming the first layer of deposited gold built of grains with a size of about a 20 nm layer thickness, the thermal resistance between the grains can be estimated to be[34]

$$R_{\mathrm{th}}=20\ \mathrm{nm}[\kappa(0)^{-1}-\kappa(\infty)^{-1}]=4\times10^{-8}\ \mathrm{m^2K/W}. \tag{5}$$

Meyer-Berg *et al.* investigated polycrystalline aluminum films with a similar technique, that produced a thermal resistance at the aluminum grain interfaces the same order of magnitude as for the resistances found here.[37]

VI. CONCLUSIONS

In summary, a photothermal microscope using the thermoreflectance technique was proved capable of micrometer resolution thermal conductivity measurements. With beam

profile analysis the thermal conductivity of a single diamond grain could be determined and a value close to that of natural IIa diamond was found. The influence of the thin surface layer of gold sputtered onto the diamond to facilitate measurements on thermal conductivity data was discussed in detail. It was shown that a film thickness of less than 30 nm has to be used to avoid coating-induced artifacts. With a similar technique the thermal conductivity of thin gold films on quartz substrates and the thermal resistance at the interface with the substrate were determined. Both exhibit a strong thickness dependence. Using a simple empirical model, we calculated the thermal resistance at the interface of grains within the gold films and found it to be in agreement with values presented by other authors.

ACKNOWLEDGMENTS

Continued encouragement and support for this work by E. Matthias and sample preparation by GEC Marconi, Towcester are gratefully acknowledged. This work was supported by Deutsche Forschungsgemeinschaft, SFB337, and by Brite EuRam under Contract No. BRE2-0154.

APPENDIX

We seek solutions of the heat diffusion equation

$$\nabla^2 T_s - \frac{1}{D_s}\frac{\partial T_s}{\partial t} = 0 \tag{A1}$$

for a thin film on a substrate system defining the temperature T_s in the substrate occupying the half space $z>0$. Assuming the film is thermally thin, i.e., assuming a constant temperature T_f throughout the film, the heat diffusion equation within the film incorporating heat exchange with the substrate at $z=0$ can be written as[24]

$$\sigma\,\frac{\partial T_f}{\partial t} = \sigma D_f \nabla_t^2 T_f + \kappa_s \frac{\partial T_s}{\partial z}, \quad \sigma = \rho_f C_{Pf} h. \tag{A2}$$

Here σ denotes the specific heat per unit area of the film with thickness h, $\rho_f C_{Pf}$ the specific heat in the film, and $\nabla_t^2 = \partial^2/\partial x^2 + \partial^2/\partial y^2$ is the two-dimensional Laplace operator. Solving Eq. (A1) together with Eq. (A2) as a boundary condition yields the substrate temperature distribution in a film/substrate system with perfect contact,[22] i.e., $T_f(x,y) = T_s(x,y,z=0)$.

A thermal contact resistance $R_{\rm th}$ between film and substrate results in a discontinuity of the temperature at the interface:

$$T_s - T_f = R_{\rm th}\kappa_s \frac{\partial T_s}{\partial z} = R_{\rm th} Q_s, \quad \text{at } z=0, \tag{A3}$$

where Q_s is the heat flux from the film to the substrate. Inserting Eq. (A3) into Eq. (A2) yields the modified boundary condition for the substrate at $z=0$

$$\sigma\left(\frac{\partial T_s}{\partial t} - \frac{\partial (R_{\rm th} Q_s)}{\partial t}\right) = \sigma D_f [\nabla_t^2 T_s - \nabla_t^2 (R_{\rm th} Q_s)] + Q_s . \tag{A4}$$

The ansatz $T = f(z)\exp[iq(x+y)/2 - i\omega t]$ for the substrate temperature yields the simple result

$$T_s = T_0 \exp(-\beta z)\exp[iq(x+y)/2]\exp(-i\omega t), \tag{A5}$$

with

$$\beta^2 = q^2 - \frac{i\omega}{D_s},$$

and an implicit equation for q

$$\frac{i\omega}{D_f} - q^2 = \frac{\kappa_s}{h\kappa_f}\,\frac{\left(q^2 - \dfrac{i\omega}{D_s}\right)^{1/2}}{1 + \kappa_s R_{\rm th}\left(q^2 - \dfrac{i\omega}{D_s}\right)^{1/2}}. \tag{A6}$$

Note that for $R_{\rm th}\to 0$ Eq. (A6) reduces to

$$\frac{i\omega}{D_f} - q^2 = \frac{\kappa_s}{h\kappa_f}\left(q^2 - \frac{i\omega}{D_s}\right)^{1/2}, \tag{A7}$$

which is identical to the condition for a film/substrate system with a perfect thermal contact at the interface. On the other hand, for $R_{\rm th}\to\infty$, Eq. (A6) simplifies to

$$q^2 = \frac{i\omega}{D_f}, \tag{A8}$$

describing the dispersion relation for the film material.

[1] L. C. Aamodt and J. C. Murphy, J. Appl. Phys. **52**, 4903 (1981).
[2] J. A. Abate and R. Roides, J. Phys. (France) Colloq. **44**, 497 (1983).
[3] E. Welsch and M. Reichling, J. Mod. Opt. **40**, 1455 (1993).
[4] A. Rosencwaig, J. Phys. (France) Colloq. **44**, 437 (1983).
[5] W. L. Smith, A. Rosencwaig, and D. L. Willenborg, Appl. Phys. Lett. **47**, 584 (1985).
[6] A. Mandelis, A. Williams, and E. K. M. Siu, J. Appl. Phys. **63**, 92 (1988).
[7] I. A. Viktin, C. Christofides, and A. Mandelis, Appl. Phys. Lett. **54**, 2392 (1989).
[8] A. M. Mansanares, D. Fournier, and A. C. Boccara, Electron. Lett. **23**, 2045 (1993).
[9] A. M. Mansanares, J. P. Roger, D. Fournier, and A. C. Boccara, Appl. Phys. Lett. **64**, 4 (1994).
[10] M. Bertolotti, G. L. Liakhou, R. L. Voti, C. Silbilia, A. Syrbu, and R. P. Wang, Appl. Phys. Lett. **65**, 2266 (1994).
[11] P. Voigt, J. Hartmann, and M. Reichling, J. Appl. Phys. **80**, 2013 (1996).
[12] S.-Y. Zhang, Z.-Q. Wang, J.-C. Cheng, Y.-S. Lu, and Y.-C. Shen, Prog. Nat. Sci. **4**, 201 (1994).
[13] G. C. Wetsel, Jr. and F. A. McDonald, Appl. Phys. Lett. **41**, 926 (1982).
[14] H. G. Walther, K. Friedrich, K. Haupt, K. Muratikov, and A. Glazov, Appl. Phys. Lett. **57**, 1600 (1990).
[15] X. D. Wu, G. S. Kino, J. T. Fanton, and A. Kapitulnik, Rev. Sci. Instrum. **64**, 3321 (1993).
[16] P. Korpiun and R. Osiander, *Photoacoustic and Photothermal Phenomena III*, Springer Series in Optical Sciences, edited by D. Bicanic (Springer, Heidelberg, 1992), Vol. 69, p. 619.
[17] J. E. Graebner, S. Jin, G. W. Kammlot, J. A. Herb, and C. F. Gardinier, Appl. Phys. Lett. **60**, 1576 (1992).
[18] D. Fournier and K. Plamann, Diam. Relat. Mater. **4**, 809 (1995).
[19] H. Verhoeven, J. Hartmann, M. Reichling, W. Müller-Sebert, and R. Zachai, Diam. Relat. Mater. **5**, 1012 (1996).
[20] H. K. Wickramasinghe, Y. Martin, D. A. H. Spear, and E. A. Ash, J. Phys. (France) Colloq. **44**, 191 (1983).
[21] R. G. Stearns, B. T. Khuri-Yakub, and G. S. Kino, Appl. Phys. Lett. **43**, 748 (1983).
[22] A. A. Maznev, J. Hartmann, and M. Reichling, J. Appl. Phys. **78**, 5266 (1995).
[23] M. Reichling, Z. L. Wu, E. Welsch, D. Schäfer, and E. Matthias, in Ref. 16, p. 698.
[24] H. S. Carslaw and J. C. Jaeger, *Conduction of Heat in Solids* (Oxford University Press, New York, 1959).
[25] M. Reichling and H. Grönbeck, J. Appl. Phys. **75**, 1914 (1994).
[26] G. Langer, J. Hartmann, and M. Reichling, Rev. Sci. Instrum. **68** (in press).

[27] J. Hartmann, P. Voigt, M. Reichling, and E. Matthias, Appl. Phys. B **62**, 493 (1996).
[28] T. R. Anthony, W. F. Bannholzer, J. F. Fleischer, L. Wie, P. K. Kuo, R. L. Thomas, and R. W. Pryor, Phys. Rev. B **42**, 1104 (1990).
[29] F. A. McDonald, Am. J. Phys. **48**, 41 (1980).
[30] J. A. Thornton, J. Vac. Sci. Technol. **12**, 830 (1975).
[31] J. A. Thornton, J. Vac. Sci. Technol. **11**, 666 (1974).
[32] J. Jauregui, Z. L. Wu, D. Schäfer, and E. Matthias, in Ref. 16, p. 682.
[33] O. W. Käding, H. Skurk, and K. E. Goodson, Appl. Phys. Lett. **65**, 1629 (1994).
[34] O. W. Käding, Ph.D. thesis, Freie Universität Berlin, Berlin, 1994.
[35] *Handbook of Chemistry and Physics*, 55th ed., edited by R. C. Weast (Chemical Rubber, Cleveland, 1974).
[36] D. W. Pashley, M. J. Stowell, M. H. Jacobs, and T. J. Law, Philos. Mag. **10**, 127 (1964).
[37] G. Meyer-Berg, R. Osiander, P. Korpium, P. Kakoschke, and H. Joswig, in Ref. 16, p. 711.